Int. J. Electrochem. Sci., 13 **(2018)** 11675 – 11683, doi: 10.20964/2018.12.08

International Journal of
ELECTROCHEMICAL
SCIENCE
www.electrochemsci.org

Short Communication

Synthesis and Pseudocapacitive Performance of Ordered Mesoporous $NiCo_2O_4$ Nanowires

Qiyue Wang[1], *Kaile Jin*[1], *Zixuan Lv*[1], *Dan Yang*[1], *Jingcai Xu*[1,2,*], *Bo Hong*[1], *Xinqing Wang*[1]

[1] College of Materials Science and Engineering, China Jiliang University, Hangzhou 310018, China
[2] College of Chemical Engineering, Zhejiang University of Technology, Hangzhou 310014, China
[*]E-mail: xujingcai@cjlu.edu.cn

Received: 16 July 2018 / *Accepted:* 31 August 2018 / *Published:* 5 November 2018

Ordered mesoporous $NiCo_2O_4$ nanowires electrodes were prepared using SBA-15 as template through a hydrothermal impregnation method. X-ray diffraction, nitrogen adsorption-desorption and transmission electron microscopy were used to characterize the structure and morphology of the SBA-15 and $NiCo_2O_4$. The pseudocapacitive performance of the samples were tested by electrochemical workstation. The results demonstrate that the ordered mesoporous $NiCo_2O_4$ electrode material exhibit excellent pseudocapacitance. The specific capacitances were calculated to be 1079.6 F g^{-1}, 1012 F g^{-1}, 943.9 F g^{-1} and 820 F g^{-1} at current densities of 1 A g^{-1}, 2 A g^{-1}, 4 A g^{-1} and 10 A g^{-1}, respectively. The cycling stability during the 1000 cycles was more than 96%. Therefore, the ordered mesoporous $NiCo_2O_4$ electrodes materials are an excellent supercapacitor electrode materials.

Keywords: Mesoporous materials; Template method; $NiCo_2O_4$; Pseudocapacitance

1. INTRODUCTION

In recent years, supercapacitors are widely used in communication, aerospace, large industrial equipment and microelectronic devices due to its high power density, short charging time and long cycle life. Supercapacitors have a broad application prospect especially in the field of new energy vehicles, which require the instant release of ultra large current [1]. According to the energy storage principle, supercapacitors are divided into electric double layer capacitor (EDLC) and pseudocapacitance. EDLC store energy with the double layer of electrode/electrolyte interface, while pseudocapacitance store energy with the rapid and reversible redox reaction on the interface. The pseudopotential capacitance is higher than the double layer capacitance, so pseudocapacitance is more potential for development [2].

The electrode materials for pseudocapacitance are mainly transition metal oxides, such as ruthenium oxide, iridium oxide, nickel oxide, cobalt oxide and manganese oxide [3-5] . Due to the advantages of high specific capacity and superior performance, the oxides of Ru and Ir are used as the electrode material of supercapacitor. However, the expensive price limits its extensive commercialization. Therefore, improving the specific capacitance of cheap transition metal oxides has become the focus of research on supercapacitors. The results showed that the performance of supercapacitor with transition bimetallic oxide ($NiCo_2O_4$, ect.) is significantly higher than that of single transition metal oxide (NiO, Co_3O_4, ect.) [6-8]. The pseudo capacitance mainly comes from the rapid reversible oxidation reduction reaction on the surface or near surface of the electrode material. According to this principle, preparation of nanoporous electrode materials is an effective way to improve pseudocapacitance. The contact area of electrode materials and electrolyte can be greatly increased by the porous nanostructure, thus increasing the utilization of electrode materials and obtaining a larger specific capacitance [9]. Previous studies have shown that the mesoporous structure with a pore size of 2~50 nm is the most suitable for supercapacitor [10]. In the study of nanoporous electrode materials, not only the pore size should be taken into account, but also the pore structure should be considered. Therefore, combined with the advantages of $NiCo_2O_4$ and ordered mesoporous materials, ordered mesoporous $NiCo_2O_4$ nanowire electrode materials are synthesized using ordered mesoporous silica (SBA-15) a hard template to by a hydrothermal impregnation method. The structure of samples were characterized by X ray diffractometer, nitrogen adsorption apparatus, thermogravimetric analysis and transmission electron microscope. The pseudocapacitive performance of the samples were tested by electrochemical workstation.

2. EXPERIMENTAL

The preparation method of SBA-15 is based on the experimental steps before [11]. The preparation steps of the ordered mesoporous $NiCo_2O_4$ nanowires are as follows: 1 g SBA-15 is put in the polytetrafluoroethylene beaker with 30ml alcohol. After being stirred evenly, 0.291 g $Ni(NO_3)_2{\cdot}6H_2O$, 0.582 g $Co(NO_3)_2{\cdot}6H_2O$ and moderate n-hexane are added into the beaker. Then stirred the mixed at 45 ℃ to the powders. The obtained powders are put into the muffle furnace to calcine at 300 ℃for 4 h. After cooling, 2mol NaOH solution is used to remove SBA-15, then washed the samples to neutral with deionized water and alcohol. After drying at 80 ℃, the ordered mesoporous $NiCo_2O_4$ nanowires are obtained.

The ordered mesoporous $NiCo_2O_4$ nanowires, conductive carbon black and 60% (W/W) polytetrafluoroethylene emulsion are mixed evenly with the mass ratio 8:1:1. A certain amount of anhydrous ethanol is added to stirred the mixed under the magnetic agitator to a slurry with a certain viscosity. The above slurry is coated on the nickel foam and pressed with 10Mpa pressure to make the coated nickel foam to a supercapacitor electrode.

The crystal structure of the sample was characterized by X ray diffraction (X-Ray Diffraction, XRD) (DX2700). The morphology of the sample was characterized by transmission electron microscopy (Transmission Eletron Microscope, TEM) (JEM-2100). The pore structure (specific

surface area and pore) of the sample was characterized by a nitrogen desorption analyzer (ASAP2020). The electrochemical performance (cyclic volt ampere characteristic, charge discharge performance and cycle life performance of the supercapacitor) were tested by the electrochemical workstation (CHI660E).

3. RESULTS AND DISCUSSION

Figure 1(a) shows the XRD wide angle diffraction pattern of mesoporous $NiCo_2O_4$. It can be seen from the diagram that the obvious diffraction peaks of $NiCo_2O_4$ appear at the 2θ of 18.9°, 31.1°, 36.7°, 38.4°, 44.6°, 55.4°, 59° and 64.9°, representing the (111), (220), (311), (222), (400), (422), (511) and (440) diffraction crystal surface of the spinel type $NiCo_2O_4$ (JCPDF NO:20-0781). This indicates that the prepared sample is $NiCo_2O_4$ with spinel structure. Meanwhile, the XRD small angle diffraction test of mesoporous SBA-15 and $NiCo_2O_4$ is carried out. From the small angle diffraction diagram of Figure 1(b), it can be seen that the obvious diffraction peaks appear at the 2θ of 0.9°, 1.55° and 1.8° for SBA-15, representing (100), (110) and (220) diffraction planes, respectively. This indicates that the SBA-15 hard template has a regular two-dimensional six party pore structure. However, the XRD small angle diffraction pattern of $NiCo_2O_4$ also shows a diffraction peak at the 2θ of 0.9°, indicating that $NiCo_2O_4$ also has a two-dimensional six square channel structure, which proves that the prepared $NiCo_2O_4$ has successfully copied the structure of SBA-15. But the small angle diffraction peak of $NiCo_2O_4$ is slightly weaker than that of SBA-15. This because when $NiCo_2O_4$ is out of SBA-15 bondage, it causes some $NiCo_2O_4$ reunite or even drill way collapse.

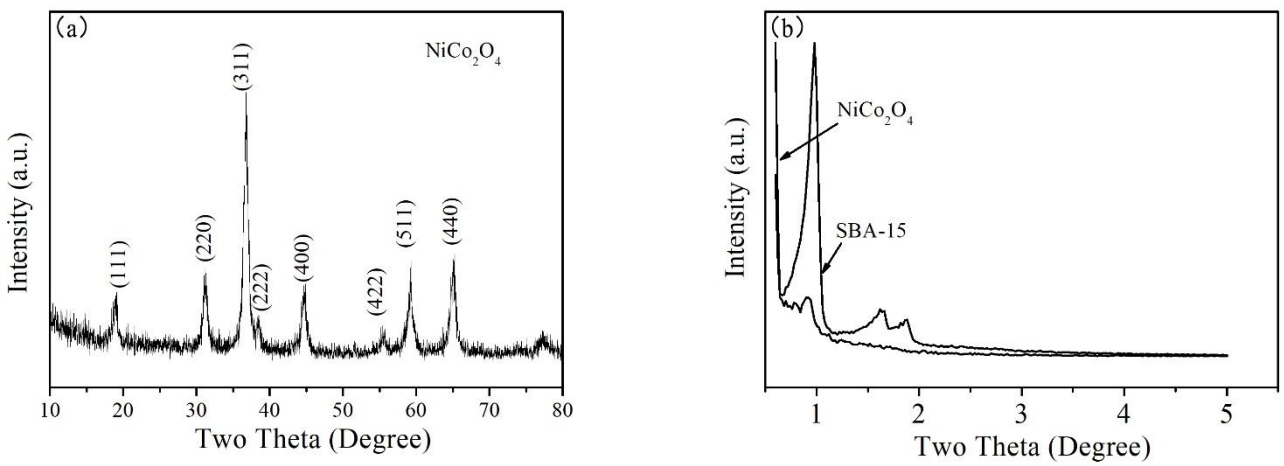

Figure 1. X-ray diffraction of samples (a) wide-angle diffraction, (b) Low-angle diffraction.

In order to further prove that the structure of ordered mesoporous $NiCo_2O_4$ is replicated effectively by the structure of the SBA-15, the morphology of SBA-15 and $NiCo_2O_4$ is characterized by TEM morphology. Figure 2 (a) shows a TEM diagram of the ordered mesoporous SBA-15. It is clear from the diagram that the prepared SBA-15 has a highly ordered two-dimensional six square

channel structure. The diameter of the uniform channel is about 6 nm and the wall thickness is about 6 nm. Figure 2 (b) shows a TEM diagram of $NiCo_2O_4$ without the SBA-15 template. It can be seen from the diagram that after removing the SBA-15 template, the morphology of the $NiCo_2O_4$ is an ordered nanowire array with diameter of about 6 nm, which further proves that the structure of the $NiCo_2O_4$ nanowire array is replicated the structure of the ordered mesoporous SBA-15.

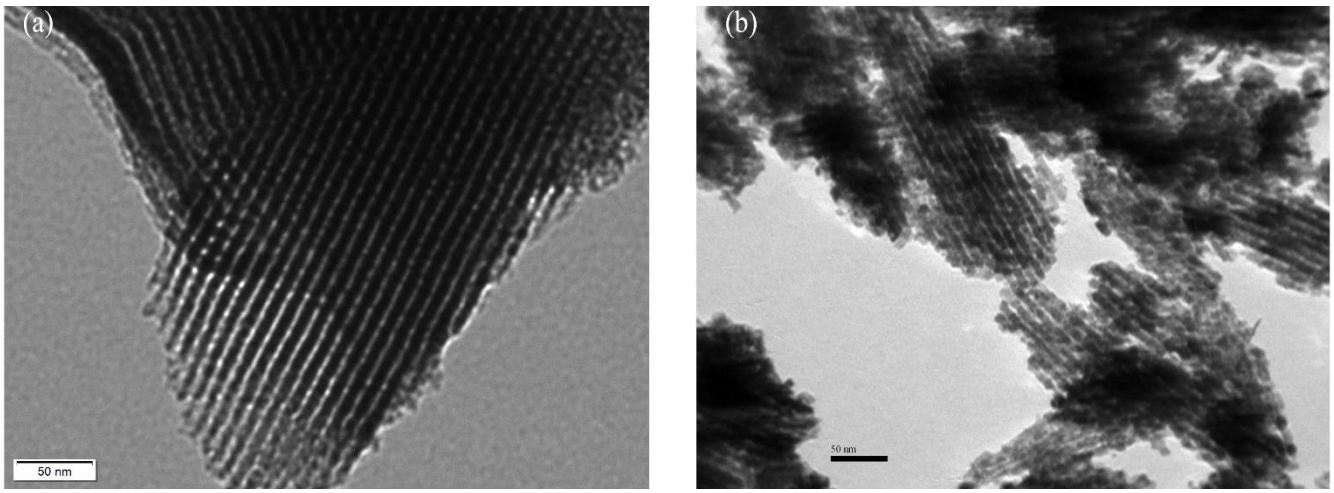

Figure 2. TEM images of (a)SBA-15 and (b)$NiCo_2O_4$.

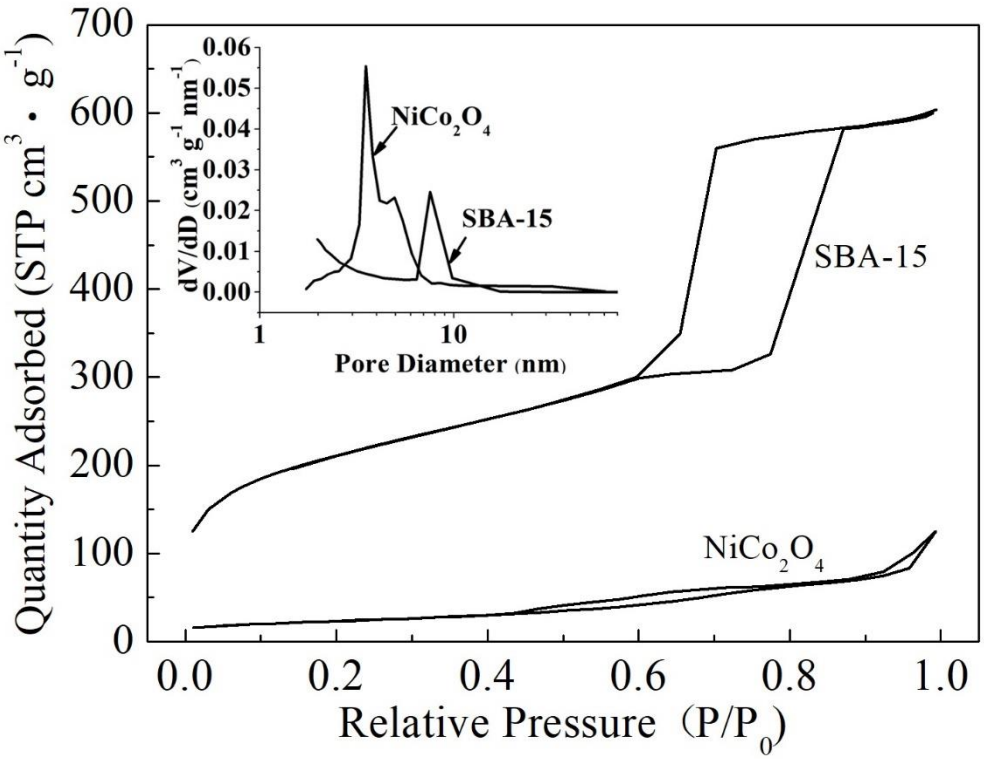

Figure 3. N_2 adsorption-desorption isotherms and pore size distribution of SBA-15 and $NiCo_2O_4$.

Table 1. Structure parameters of SBA-15 and $NiCo_2O_4$

Material	BET surface area ($m^2 \cdot g^{-1}$)	Total pore volume ($m^3 \cdot g^{-1}$)	Pore size (nm)
SBA-15	755.7	0.90	6.1
$NiCo_2O_4$	80.2	0.19	3.8

Figure 3 shows a N_2 adsorption-desorption diagrams of SBA-15 and $NiCo_2O_4$. It is shown from the diagram that the adsorption-desorption isotherm curve of SBA-15 shows a typical type IV isothermal adsorption curve with a typical H1 type hysteresis loop, which indicates that the prepared SBA-15 is an ordered mesoporous material. It can be seen from the pore size distribution that the most probable pore diameter of SBA-15 is 6 nm. The specific surface area, pore volume and average pore size of SBA-15 are calculated according to the adsorption curve. The specific parameters are shown in Table 1. The specific surface area of SBA-15 is 755.7 m^2/g, the total pore volume is 0.90 m^3/g and the average pore size is 6.1 nm. It can be seen that SBA-15 has a relatively large specific surface area, and has a mesoporous pore size distribution (average 6.1 nm, consistent with TEM analysis). It is an excellent template material. The N_2 adsorption desorption diagram and the pore size distribution of $NiCo_2O_4$ can be seen that the mesoporous $NiCo_2O_4$ adsorption isotherm of the crystalline state retained the typical IV curve with H1 type hysteresis loop of SBA-15. Again, the ordered mesoporous $NiCo_2O_4$ replicates the mesoporous structure of SBA-15. But the hysteresis loop of $NiCo_2O_4$ is more flat and narrower than that of SBA-15. This because the $NiCo_2O_4$ lose the support of the template after removing the SBA-15 template, resulting in the $NiCo_2O_4$ reunion and the collapse of the channel, which can be seen from the TEM diagram of $NiCo_2O_4$.

The specific surface area, pore volume and average pore diameter of $NiCo_2O_4$ material are calculated according to the adsorption curve. The specific parameters are shown in Table 1. It can be seen from the table that the specific surface area of $NiCo_2O_4$ is 80.2 m^2/g, the total pore volume is 0.19 m^3/g, the average pore size is 4.8 nm. The specific surface area, the total pore volume and the average pore size of $NiCo_2O_4$ are significantly lower than that of SBA-15. According to the TEM diagram， the size of the aperture of SBA-15 is about 6 nm and the thickness of the wall is about 6nm, while the pore size of the mesoporous $NiCo_2O_4$ should be about 6 nm and the wall thickness is about 6nm. But, in fact, the average pore size calculated according to the adsorption curve is 3.8 nm, which explains the partial aggregation of the mesoporous $NiCo_2O_4$ and the collapse of the pore. But in general, most of $NiCo_2O_4$ retained the ordered mesoporous structure of SBA-15.

Figure 4 (a) shows a cyclic voltammetric diagram of the $NiCo_2O_4$ electrode material. It can be found from the diagram that the electrode materials show good cyclic volt ampere pseudopotential characteristics. The obvious redox peaks appear at the potential of 0.2 V and 0.45 V, representing the redox peaks of Co^{3+}/Co^{2+} and Ni^{3+}/Ni^{2+}. The corresponding redox reactions are based on the following equations: $NiCo_2O_4 + OH^- \text{——} NiCo_2O_4 \mid\mid OH^- + NiCo_2O_4\text{-}OH$. With the the scanning rate gradually increasing from 5 mv/s to 40 mv/s, the redox peaks of Co^{3+}/Co^{2+} and Ni^{3+}/Ni^{2+} take a positive or negative displacement. It indicates the quasi reversibility of the electrode reaction and the pseudo capacitance behavior of the electrode material.

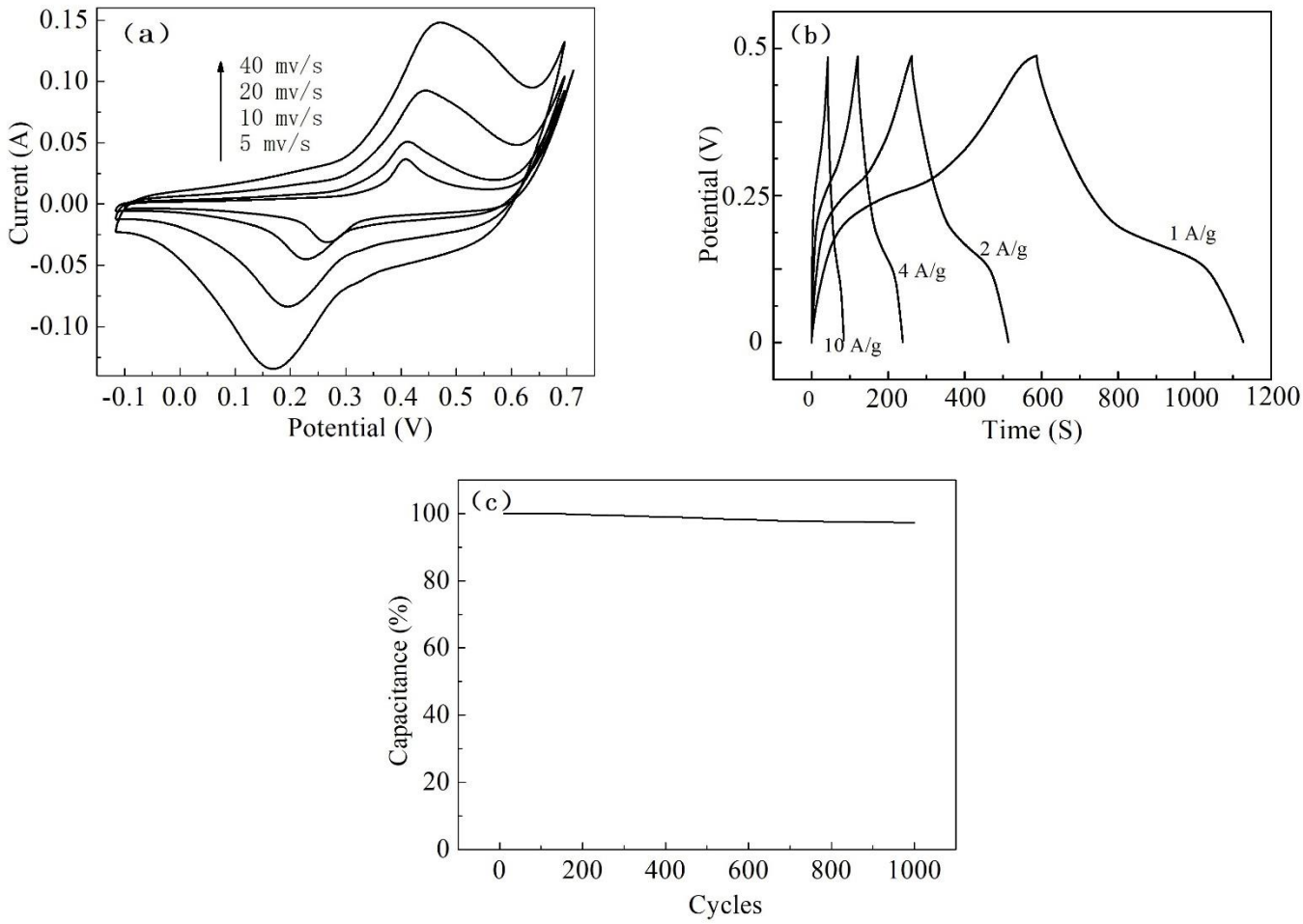

Figure 4. Pseudocapacitive performance of $NiCo_2O_4$: (a) CV curves, (b) GCD curves, (c)Cycling stability.

Figure 4 (b) shows the charge discharge curves at current density of 1 A g^{-1}, 2 A g^{-1}, 4 A g^{-1} and 10 A g^{-1}. It can be seen from the diagram that the potential changes of all charging and discharging curves are not linear. The obvious potential change inflection point are the same with the redox peak potential of the cyclic voltammetry curve. This again illustrates that the redox reaction is the main contribution of electrode materials to pseudo capacitance behavior. According to the discharge curve, the specific capacitance of the electrode material is calculated with the formula: $C=(i*\triangle t)/(m*\triangle V)$. The i is the discharge current, $\triangle t$ is the discharge time, m is the quality of electrode materials, $\triangle V$ is the change of potential. The specific capacitance values of the ordered mesoporous $NiCo_2O_4$ electrode materials are 1079.6 F g^{-1}, 1012 F g^{-1}, 943.9 F g^{-1} and 820 F g^{-1} at 1 A g^{-1}, 2 A g^{-1}, 4 A g^{-1} and 10 A g^{-1}, respectively. Apparently, the as-synthesized $NiCo_2O_4$ electrode materials delivers a much higher specific capacitance than various architectures $NiCo_2O_4$ based electrode materials, such as $NiCo_2O_4$ nanoplates (294 F g^{-1} at 1 A g^{-1}) [12], thin-film (575 F g^{-1} at 1 A g^{-1}) [13], nanoflakes (490 F g^{-1} at 15 A g^{-1}) [14], nanorods (330 F g^{-1} at 15 A g^{-1}) [14], hexagonal (663 F g^{-1} at 15 A g^{-1}) [15]. Figure 4 (c) shows a specific capacitance value diagram of its 1000 cycles. It can be seen from the diagram that an ordered mesoporous $NiCo_2O_4$ electrode still maintains a specific capacitance of more than 96% over

1000 cycles at the 10 A g^{-1} current density. Furthermore, the as-synthesized $NiCo_2O_4$ electrode materials shows an enhanced cycle life at high current density compared to various $NiCo_2O_4$ based electrode materials. The comparison of electrochemical performances of the $NiCo_2O_4$ prepared in other previous reports and present work are listed Table 2 [12-22]. Wu [16] and Chen[17] have proved that the porous structures of $NiCo_2O_4$ provide more diffusion paths for the electrolyte transport, which are benefical for the fast diffusion of electrolyte ions transmission in the electrolyte, increasing the cycle life at high current density. However, in present work, the specific capacitance values and cycle life are much better. This because the ordered mesoporous structures of $NiCo_2O_4$, which could provide the larger specific surface area and much appropriate pore size for the affluent adsorption and fast diffusion of electrolyte ions transmission in the electrolyte, resulting the higher specific capacitance and excellent cycle life. So the ordered mesoporous $NiCo_2O_4$ materials is an excellent electrode material for supercapacitors.

Table 2. Comparison of the electrochemical performances of the as-prepared $NiCo_2O_4$ with the other published results.

Materials	Methods	Specific capacitance (F g^{-1})	Rate performance	Capacity retention	Reference
$NiCo_2O_4$ nanoplates	Hydrothermal and calcination	294 (1 A g^{-1})	48% (10 A g^{-1})	89.8% (2200 cycles)	12
$NiCo_2O_4$ thin-film	Electrochemically	575 (1 A g^{-1})	98% (10 A g^{-1})	99% (1000 cycles)	13
$NiCo_2O_4$ nanoflakes	Chemical bath deposition	490 (15 A g^{-1})	No data	97% (900 cycles)	14
$NiCo_2O_4$ nanorods	Chemical bath deposition	330 (15 A g^{-1})	No data	96% (900 cycles)	14
$NiCo_2O_4$ hexagonal	Hydrothermal and calcination	663 (1 A g^{-1})	88% (8 A g^{-1})	88.4% (5000 cycles)	15
$NiCo_2O_4$	Sol–gel approach	222 (1 A g^{-1})	84% (3.5 A g^{-1})	96.3% (600 cycles)	16
Porous $NiCo_2O_4$	Hydrothermal and annealing route	658 (1 A g^{-1})	78% (20 A g^{-1})	93.5 (1000 cycles)	17
$NiCo_2O_4$	Combustion	429.6 (1 A g^{-1})	74% (16 A g^{-1})	88% (4000 cycles)	18
$NiCo_2O_4$ hexagonal	Rotary evaporat	568.0 (1 A g^{-1})	71% (16 A g^{-1})	76.8% (2000 cycles)	19

$NiCo_2O_4$ nanoneedle	Hydrothermal route	0.988C cm^{-2} (2mA cm^{-2})	60% (200mA cm^{-2})	80.7% (12000 cycles)	20
Bilayer $NiCo_2O_4$	Solution based	2363 (0.5 A g^{-1})	61.5% (8 A g^{-1})	77.5% (1000 cycles)	21
$NiCo_2O_4$ nanosphere	Hydrothermal and calcination	1229 (1 A g^{-1})	83.6% (25 A g^{-1})	86.3% (3000 cycles)	22
Ordered mesoporous $NiCo_2O_4$	Hydrothermal impregnation method	1079.6 (1 A g^{-1})	76%(10 A g^{-1})	96% (1000 cycles)	This work

4. CONCLUSION

In this paper, ordered mesoporous silica (SBA-15) was used as a hard template to synthesize ordered mesoporous $NiCo_2O_4$ nanowires electrode materials by hydrothermal impregnation method. The structures and pseudocapacitance performance of ordered mesoporous $NiCo_2O_4$ nanowires were tested. The results show that the specific capacitance values were 1079.6 F g^{-1}, 1012 F g^{-1}, 943.9 F g^{-1} and 820 F g^{-1} at current densities of 1 A g^{-1}, 2 A g^{-1}, 4 A g^{-1} and 10 A g^{-1}, respectively. The specific capacitance was still above 96% after 1000 cycles at the 10 A g^{-1}. The ordered mesoporous $NiCo_2O_4$ nanowires electrode materials exhibit excellent pseudo capacitance properties.

ACKNOWLEDGMENTS
The research was funded by the Foundation of Science and Technology Department of Zhejiang Province (No. 2017C37067, 2017C33078) and Technology Innovation Plan and Planted Talent of College students of Zhejiang Province (2018R409015).

References

1. A. González, E. Goikolea, J. A. Barrena and R. Mysyk, *Sust. Energ. Rev.*, 58 (2016) 1189.
2. W. Zuo, R. Li, C. Zhou, Y. Li, J. Xia and J. Liu, *Adv. Sci.*, 4 (2017) 1600539.
3. Q. Lu, J. G. Chen, J. Q. Xiao, *Angew. Chem. Int. Ed.*, 52 (2013) 1882.
4. G. Zhang, X. Xiao, B. Li, P. Gu, H. Xue and H. Pang, *J. Mater. Chem. A*, 5 (2017) 8155.
5. M. Huang, F. Li, F. D. Yu, Y. X. Zhang and L. Li, *J. Mater. Chem.* ., 3 (2015) 21380.
6. D. Chen, Q. Wang, R, Wang and G. Shen, *J. Mater. Chem. A*, 3 (2015) 10158.
7. K. M. Deng, L. Li, *Funct. Mater. Lett.,* 8 (2015) 1530002.
8. C. Wang, E. Zhou, W. He, X. Deng, J. Huang, M. Jing, X. Wei, X. Liu and X. J. Xu, *Nanomaterials*, 7 (2017) 41.
9. C. Guan, X. Li, Z. Wang, X. Cao, C. Soci, H. Zhang and H. J. Fan, *Adv. Mater.*, 24 (2012) 186.
10. T. Brezesinski, J. Wang, S. H. Tolbert and B. Dunn, *Nat. Mater.*, 9 (2010) 146.
11. X. Q. Wang, M. Chen, L. Li, D. Jin, H. Jin and H. Ge, *Mater. Lett.*, 64 (2010) 708.
12. J. Pu, J. Wang, X. Q. Jin, F. Cui, E. H. Sheng and Z. H. Wang, *Electrochim. Acta,* 106 (2013) 226.
13. V. Gupta, S. Gupta and N. Miura, *J. Power. Sources,* 195 (2010) 3757.
14. R. R. Salunkhe, K. Jang, H. Yu, S. Yu, T. Ganesh, S. H. Han and H. Ahn, *J. Alloys. Compd.,* 509

(2011) 6677.
15. J. Pu, X. Q. Jin, J. Wang, F. L. Cui, S. B. Chu, E. H. Sheng and Z. H. Wang, *J. Electroanal. Chem.,* 707 (2013) 66.
16. Y. Q. Wu, X. Y. Chen, P. T. Ji and Q. Q. Zhou, *Electrochim. Acta,* 56 (2011) 7517.
17. H. Chen, J. Jiang, L. Zhang, T. Qi, D. Xia and H. Wan, *J. Power Sources,* 248 (2014) 28.
18. T. Huang, B. Liu, P. Yang, Z. Qiu and Z. Hu, *Int. J. Electrochem. Sci.,* 13 (2018) 6144.
19. B. Zhang, J. Zhu, H. Liu, P. Shi, W. Wu, F. Wang and Y. Liu, *Ceram. Int.,* 44 (2018) 8695.
20. C. Liu, W. Jiang, F. Hu, X. Wu and D. Xue, *Inorg. Chem. Front.,* 5 (2018) 835.
21. S. Wu, F. Xue, M. Wang, and J. Wang, *Integr. Ferroelectr.,* 189 (2018) 158.
22. K. Xu, J. Yang, J. Hu, *J. Colloid. Interf. Sci.,* 511 (2018) 456.